Available online at www.sciencedirect.com

ScienceDirect

International Journal of Naval Architecture and Ocean Engineering 8 (2016) 38–52
http://www.journals.elsevier.com/international-journal-of-naval-architecture-and-ocean-engineering/

Application of neuro-fuzzy algorithm to portable dynamic positioning control system for ships

Ming-Chung Fang, Zi-Yi Lee*

National Cheng Kung University, Taiwan, ROC

Received 30 December 2014; revised 31 March 2015; accepted 15 September 2015
Available online 19 January 2016

Abstract

This paper describes the nonlinear dynamic motion behavior of a ship equipped with a portable dynamic positioning (DP) control system, under external forces. The waves, current, wind, and drifting forces were considered in the calculations. A self-tuning controller based on a neuro-fuzzy algorithm was used to control the rotation speed of the outboard thrusters for the optimal adjustment of the ship position and heading and for path tracking. Time-domain simulations for ship motion with six degrees of freedom with the DP system were performed using the fourth-order Runge–Kutta method. The results showed that the path and heading deviations were within acceptable ranges for the control method used. The portable DP system is a practical alternative for ships lacking professional DP facilities.

Keywords: Dynamic positioning; Pipe laying; Neuro-fuzzy; Short-crested waves

1. Introduction

In ocean engineering, dynamic positioning (DP) is required for purposes such as pipe laying, offshore wind farm, and methane clathrate extraction. Because of external forces, the position and velocity of ships can deviate from the planned position and velocity, and consequently, ships might encounter DP problems during the working process, especially because of limitations on the use of anchor chains. Therefore, systems for maintaining a stable position and heading are required.

The first DP system, developed in the 1960s (Fay, 1989), involved a single-input single-output proportional–integral–derivative (PID) controller and was designed for controlling the horizontal motion of a plane (surge, sway, and yaw). Through appropriate adjustment, the PID controller of the DP system is typically effective in the concerned sea state. However, the control efficiency may be low for a different sea state or at certain ship speeds.

Generally, vessels controlled by DP systems have different types of thrusters, such as azimuth thrusters, propulsion propellers with rudders, for generating forces for maintaining the desired position and heading in the horizontal plane (Morgan, 1978; Zalewski, 2011). DP systems involving different control techniques based on linear optimal and Kalman filter theories have been used in ships to overcome DP problems (Balchen et al., 1980; Sørensen et al., 1996). However, the Kalman filter should generally be combined with another analytical technique in practice (Saelid et al., 1983). Lee et al. (2002) developed a DP system based on the fuzzy theory, and it was used for the control outputs, including the rudder angle, propeller thruster, and a lateral bow thruster, to counteract environmental forces. Tannuri and Donha (2000) developed a controller design methodology for a DP system for floating production storage and offloading vessels in deep water. Perez and Donaire (2009) proposed a design that combined position and velocity loops in a multivariable anti-windup implementation. Sørensen (2011) showed that using PID controllers

* Corresponding author.
E-mail address: z10301066@email.ncku.edu.tw (Z.-Y. Lee).
Peer review under responsibility of Society of Naval Architects of Korea.

http://dx.doi.org/10.1016/j.ijnaoe.2015.09.003

for output feedback control, nonlinear control, or hybrid control could improve the performance and operability of onboard DP systems, rendering the ship suitable for a variety of missions and environments.

The aforementioned references focused on two types of ships: (1) professional vessels equipped with DP systems at the initial design stage and (2) ships without DP devices, that use the rudder to control the thrust vector. The objective of the present study was to use automatic controllers as a portable DP system for controlling the outboard thrusters in vessels without a DP system, e.g., barges.

The proposed DP system that consists of portable thruster is similar to the DP system developed by Thrustmaster of Texas Inc. in 1988 (Maritime Reporter, 2002). However, costly azimuth thrusters are used in the product of Thrustmaster of Texas Inc., whereas general propeller thrusters, which are more economical, were adopted in the present study. Furthermore, because the DP control algorithm of Thrustmaster of Texas Inc. has not been released to the public, the present study attempted to develop a DP system with optimal control based on a neuro-fuzzy algorithm.

For a controller to show high performance, its system parameters should be adjusted in a timely manner. However, parameter optimization would require considerable time and present difficulties if a trial-and-error method were to be used. To achieve high efficiency, the related control parameters are automatically adjusted using adaptive control.

A fuzzy control model with the structure of adaptive networks is called adaptive-network-based fuzzy inference system (ANFIS) (Jang and Sun, 1995), and it is simply called neuro-fuzzy algorithm in this paper. It has the merits of self-tuning by using a neural network algorithm, and intuitional system adjustment through fuzzy control. Furthermore, both fuzzy control and neural network algorithms do not require a mathematical model for deriving the controller, which saves the time that would otherwise be required for constructing the model. ANFIS involves a neural network algorithm based on fuzzy control. The fuzzy rule base and membership functions can be adjusted during the learning process of the adaptive network (Cheng, 2000).

A fuzzy inference system can not only accept linguistic information (fuzzy rules) from human experts or knowledge, but also adjust the system parameters by using the training data to achieve better control performance. This capability leads to fuzzy inference systems having an advantage over individual neural network algorithms, which cannot preselect the control rule directly.

The equations used for simulating the time-domain motion responses of a ship on waves consist of a combination of a nonlinear equation for six degrees of motion (Hamamoto et al., 1994) and the derivatives of maneuver and thruster forces. To simulate a real sea environment, short-crested waves, ocean currents, wind, and second-order drifting forces are also considered in the simulations. The nonlinear mathematical model of Fang and Luo (2005), which considers seakeeping and maneuvering characteristics, consists of a set of ordinary differential equations (ODEs). These equations are required to determine the six-degree-of-freedom (six-DOF) motions of a barge in random waves. The fourth-order Runge–Kutta method was applied to solve the ODEs for time-domain motion simulations. The proposed portable DP system consisting of thrusters, whose rotation speed is controlled by using a neuro-fuzzy algorithm, generates forces to counteract environmental forces.

Because an appropriate and professional ship equipped with a DP system is rare and costly, identifying alternatives to a sophisticated DP system is necessary. Moreover, many ships may not have originally been equipped with a DP system, and therefore, the use of portable outboard thrusters as a DP system, as suggested by the present study, could be an effective alternative.

2. Mathematical models

The mathematical model can be described in three coordinate systems, as illustrated in Fig. 1: the earth-fixed coordinate system $O-X_0Y_0Z_0$, ship body coordinate system $G-xyz$, and horizontal body coordinate system $G-x'y'z'$. The coordinates of the center of gravity of the ship in the $O-X_0Y_0Z_0$ coordinate system are represented by X_G, Y_G, and Z_G, and Euler's angles are denoted by ϕ, θ, and ψ.

In this study, nonlinear equations based on the mathematical model of Fang and Luo (2005) were used to describe dynamic ship motion responses to external forces in the ocean. The nonlinear equations describing six-DOF ship motions under DP control are as follows:

$$\begin{aligned} m(\dot{u}-v\dot{\psi}) = {} & (m_y - X_{v\dot{\psi}})v\dot{\psi} - m_x\dot{u} - m_x z_G\ddot{\theta} - m_z w\dot{\theta} + X_{FK} \\ & + X_{WF} - R + X_D + F_{cx} + F_{Tx} \\ & - F_{cable} \quad \text{(surge motion)} \end{aligned} \tag{1}$$

$$\begin{aligned} m(\dot{v}+u\dot{\psi}) = {} & -m_x u\dot{\psi} - m_y\dot{v} + m_y z_G\ddot{\phi} - Y_v v - Y_{\dot{\psi}}\ddot{\psi} + Y_{\dot{\psi}}\dot{\psi} \\ & + Y_{v|v|}v|v| + Y_{v|\dot{\psi}|}v|\dot{\psi}| + Y_{\dot{\psi}|\dot{\psi}|}\dot{\psi}|\dot{\psi}| + Y_{FK} + Y_{DF} \\ & + Y_{WF} + Y_D + F_{cy} + F_{Ty} \quad \text{(sway motion)} \end{aligned} \tag{2}$$

$$\begin{aligned} m\dot{w} = {} & -m_z\dot{w} - Z_w w - Z_{\ddot{\theta}}\ddot{\theta} - Z_{\dot{\theta}}\dot{\theta} - Z_\theta\theta + Z_{FK} + Z_{DF} \\ & + mg \quad \text{(heave motion)} \end{aligned} \tag{3}$$

$$\begin{aligned} I_{xx}\ddot{\phi} - I_{xx}\dot{\theta}\dot{\psi} = {} & J_{xx}\dot{\theta}\dot{\psi} - J_{xx}\ddot{\phi} - K_{\dot{\phi}}\dot{\phi} + m_y z_G\dot{v} + (Y_v v - Y_{\dot{\psi}}\dot{\psi})z_G \\ & + K_{FK} + K_{DF} + K_{WF} + N_{Tx} \quad \text{(roll motion)} \end{aligned} \tag{4}$$

$$\begin{aligned} I_{yy}\ddot{\theta} + I_{xx}\dot{\psi}\dot{\phi} = {} & -J_{xx}\dot{\phi}\dot{\psi} - J_{yy}\ddot{\theta} - M_{\dot{\theta}}\dot{\theta} - M_\theta\theta - M_{\dot{w}}\dot{w} - M_w w \\ & - m_x z_G\dot{u} + M_{FK} + M_{DF} + N_{Ty} \quad \text{(pitch motion)} \end{aligned} \tag{5}$$

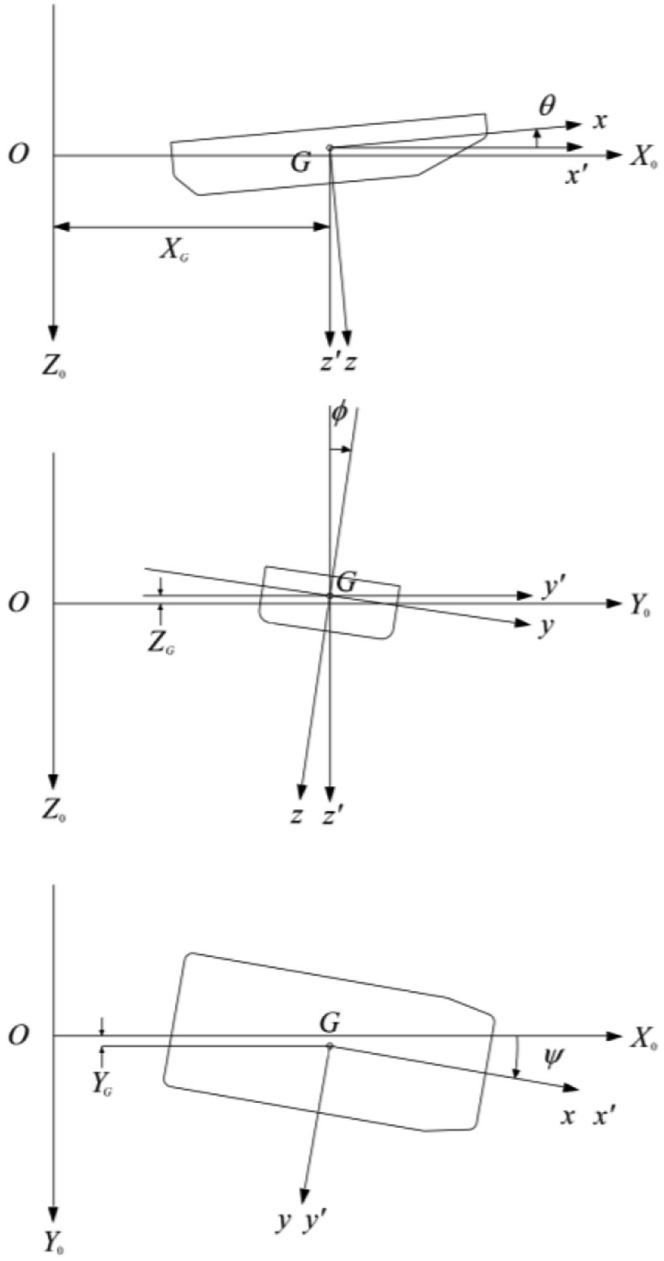

Fig. 1. Coordinate systems.

$$
\begin{aligned}
I_{zz}\ddot{\psi} - I_{xx}\dot{\theta}\dot{\phi} = {} & J_{xx}\dot{\theta}\dot{\phi} - J_{zz}\ddot{\psi} - N_{\dot{v}}\dot{v} - N_v v - N_{\dot{\psi}}\dot{\psi} + N_{\dot{\psi}|\dot{\psi}|}\dot{\psi}|\dot{\psi}| \\
& + N_{vv\dot{\psi}}v^2\dot{\psi} + N_{v\dot{\psi}\dot{\psi}}v\dot{\psi}^2 + N_{\phi}\phi + N_{v|\phi|}v|\phi| \\
& + N_{\dot{\psi}|\phi|}\dot{\psi}|\phi| + \Big(- Y_v v + Y_{\dot{\psi}}\dot{\psi} + Y_{v|v|}v|v| \\
& + Y_{v|\dot{\psi}|}v|\dot{\psi}| + Y_{\dot{\psi}|\dot{\psi}|}\dot{\psi}|\dot{\psi}| \Big) x_H + N_{FK} + N_{DF} \\
& + N_{WF} + N_D + N_C + N_{Tz} \quad \text{(yaw motion)}
\end{aligned} \tag{6}
$$

where m is the ship mass; m_x, m_y, and m_z are the ship added masses in the directions of the x-, y- and z-axis; I_{xx}, I_{yy}, and I_{zz} are the mass moments of inertia about the three rotation axes; J_{xx}, J_{yy}, and J_{zz} are the ship added mass moments of inertia about the three rotation axes; u, v, and w are the surge, sway, and heave velocities of the ship in coordinate system $G{-}x'y'z'$, respectively; ϕ, θ, and ψ are the roll, pitch, and yaw displacements, respectively; and g is the acceleration of gravity. In Eqs. (3) and (5), the seakeeping coefficients of the heave and pitch motion can be obtained through the Frank close-fit method (Fang et al., 1993; Luo, 2001); x_H and z_H are the points of application of hydrodynamic force in the sway mode, and they correspond to the longitudinal and vertical coordinates of the ship's center of gravity. In Eqs. (1)–(6), X, Y, and Z represent external forces in the surge, sway, and heave directions, respectively, and K, M, and N are the external moments in the roll, pitch, and yaw directions, respectively. The subscripts FK and DF represent the Froude–Krylov force and diffraction force, which are exerted by waves; the subscript WF represents the wind force; R is the resistance of the ship; X_D, Y_D, and N_D are the longitudinal drifting force, lateral drifting force, and drifting moment in short-crested waves, respectively; F_{cx} and F_{cy} are the current forces; N_c is the current moment; F_{Tx} and F_{Ty} are the thruster forces produced by the DP system for the surge and sway, respectively; N_{Tx}, N_{Ty}, and N_{Tz} are the thruster moments produced by the DP system for the roll, pitch, and yaw, respectively; and F_{cable} is the cable force in pipe-laying simulations. Details of the methods used and calculations performed for determining the aforementioned external forces and moments are provided in the subsequent sections. For the definitions and derivations of the rest of the variables in Eqs. (1)–(6), the reader is referred to the paper of Luo (2006).

3. Short-crested waves

The wave energy spectral analysis theory can be used to model a realistic irregular wave field as a function of the sea state. In this study, to realistically simulate ship motions, the wave forces were calculated for short-crested waves, which are obtained by superimposing many regular waves with different directions of motion.

The wave spectrum and corresponding spreading function based on International Towing Tank Conference (ITTC)-1978 (Michel, 1999; ITTC, 2005) are as follows:

$$
S_{aa}(\omega_i) = \frac{172.75H_{1/3}^2}{\overline{T}^4\omega_i^5}\exp\left(\frac{-691}{\overline{T}^4\omega_i^4}\right) \tag{7}
$$

$$
S_{aa}(\omega_i,\mu_j) = S_{aa}(\omega_i) \times \frac{2}{\pi}\cos^2\mu_j \tag{8}
$$

where $H_{1/3}$ is the significant wave height. The characteristic wave period $\overline{T}$ is typically considered as the zero-crossing period $\overline{T}_Z$ (Phelps, 1995). Furthermore, ω_i is the frequency of the ith regular wave, and μ_j is the angle between the jth wave direction and the dominant wave direction. The angle

ranges are defined as $\left(-\frac{\pi}{2}<\mu_j<\frac{\pi}{2}\right)$. To approach the real wave pattern and avoid the repeated wave pattern, the simulation of irregular waves and superimposing it with appropriate numbers of regular wave components is necessary. However, if too many wave components are selected for every direction, the computation time required would increase considerably. Therefore, every two-dimensional irregular wave is constructed from 20 regular wave components with the same direction, and the short-crested waves consist of two-dimensional irregular waves from 13 wave directions.

The resultant diffraction force acting on the ship body can be obtained. For short-crested waves built from regular waves, the corresponding encounter frequency should be determined for calculating the added mass and damping coefficients. In practice, the damping coefficients for the case of the ship sailing in irregular waves can be obtained from the average frequency $\overline{\omega}$ of the spectrum (Crossland and Johnson, 1998):

$$\overline{\omega}=0.5\left(\frac{2\pi}{1.296\overline{T}}+\sqrt{\frac{2\pi g}{1.25L}}\right) \tag{9}$$

where $\overline{T}$ is the characteristic wave period and L is the ship length.

4. Mean drifting force

While the ship is moving on waves, additional nonlinear hydrodynamic forces, the additional resistance, and lateral drifting forces act on the ship hull. The added resistance is the longitudinal component of the resistance and directly contributes to the ship's deceleration. The lateral drifting forces act in the transverse direction and cause the ship to deviate from its path. Under the weak scatterer assumption, the nonlinear hydrodynamic forces can be obtained by using the technique employed by Salvesen (1974):

$$F(\omega_e)=R_e\left\{-\frac{1}{2}\rho\iint_{S_B}\left[\phi_B\frac{\partial}{\partial n}-\frac{\partial\phi_B}{\partial n}\right]\nabla\phi_I^* ds\right\} \tag{10}$$

This equation considers only the horizontal component, ϕ_I^* is the complex conjugate of the incident wave potential ϕ_I, and ϕ_B is the ship body disturbance potential obtained from strip theory. The integral is around the ship body surface S_B. Generally, the nonlinear hydrodynamic force, which is calculated in the frequency domain, is represented as a mean value (i.e., mean nonlinear hydrodynamic force) in the following equation (Fang, 1991), which is a modified form of Eq. (10):

$$F(\omega_e)=\mathrm{Re}\left\{\frac{i}{2}\rho K_0\left[\iint_{S_B}\left(\sum_{m=2}^{6}S^m\phi_R^m+\phi_D\right)\frac{\partial}{\partial n}\phi_I^* ds-\iint_{S_B}\left(\frac{\partial}{\partial n}\left(\sum_{m=2}^{6}S^m\phi_R^m+\phi_D\right)\right)\phi_I^* ds\right]\right\}\left(\cos\psi\,\vec{i}+\sin\psi\,\vec{j}\right) \tag{11}$$

where S^m is the jth motion mode; the values 2, 3, 4, 5, and 6 of the subscript j represent the sway, heave, roll, pitch, and yaw, respectively; and ϕ_R^m and ϕ_D are the radiation wave potential and the diffraction wave potential, respectively. In Eq. (11), the surge motion is assumed to be small and is therefore neglected.

In the present study, for short-crested waves, the mean longitudinal and lateral drifting forces acting on the ship with respect to the wave heading ψ can be written as

$$\overline{F}_D=2\int_{-\frac{\pi}{2}}^{\frac{\pi}{2}}\int_{0}^{\infty}\frac{F(\omega)}{a^2}S_{aa}(\omega,\mu)\cdot d\omega d\mu \tag{12}$$

$$X_D=\left|\overline{F}_D\right|\cos\psi \tag{13}$$

$$Y_D=\left|\overline{F}_D\right|\sin\psi \tag{14}$$

where $\overline{F}_D$ is the mean nonlinear hydrodynamic force acting on the ship when the ship is on random waves, $S_{aa}(\omega,\mu)$ is the ITTC-1978 wave spectrum, and a is the wave amplitude. The parameter N_D can be integrated from the sectional Y_D with respect to the longitudinal center of gravity (LCG) along the entire ship length. Related introduction can be obtained from the paper of Fang et al. (2013).

5. Wind forces

Estimates of the wind forces and moments on the ship are based on the formulas developed by Isherwood (1973):

$$X_{WF}=X_W(\gamma_R)\frac{1}{2}\rho_a A_f V_R^2 \tag{15}$$

$$Y_{WF}=Y_W(\gamma_R)\frac{1}{2}\rho_a A_S V_R^2 \tag{16}$$

$$K_{WF}=K_W(\gamma_R)\frac{1}{2}\rho_a\left(\frac{A_S^2}{L}\right)V_R^2 \tag{17}$$

$$N_{WF}=N_W(\gamma_R)\frac{1}{2}\rho_a A_S L V_R^2 \tag{18}$$

where X_{WF}, Y_{WF}, K_{WF}, and N_{WF} are the wind forces and moments in the surge, sway, roll, and yaw directions, respectively; X_W, Y_W, K_W, and N_W are nondimensional coefficients of the wind forces and moments with respect to the relative wind angle γ_R; and ρ_a is the air density. The parameters A_f and A_S are the longitudinal and sideward projected areas of the ship hull above the water surface, respectively, and V_R is the relative speed between the ship and the wind. Furthermore, K_W is generally small and can be neglected (Isherwood, 1973).

6. Ocean current forces

The current forces and moment on the ship are related to the relative speed and direction between the ship and the current, and they can be expressed as

$$F_{cx} = \frac{1}{2}\rho\left[(V_c\cos\alpha - \dot{x}_G)^2 + (V_c\sin\alpha - \dot{y}_G)^2\right]BdC_{cx} \tag{19}$$

$$F_{cy} = \frac{1}{2}\rho\left[(V_c\cos\alpha - \dot{x}_G)^2 + (V_c\sin\alpha - \dot{y}_G)^2\right]L_{pp}dC_{cy} \tag{20}$$

$$N_c = \frac{1}{2}\rho\left[(V_c\cos\alpha - \dot{x}_G)^2 + (V_c\sin\alpha - \dot{y}_G)^2\right]L_{pp}^2dC_{cn} \tag{21}$$

where V_c is the current speed, α is the angle between the current and the ship heading, $\dot{x}_G$ and $\dot{y}_G$ are the horizontal components of the ship speed with respect to the center of gravity, and L_{pp} is the ship length between the perpendiculars. The corresponding coefficients C_{cx}, C_{cy}, and C_{cn} are nondimensional coefficients of the forces and moment with respect to α and obtained from empirical formulas (Nienhuis, 1986).

7. Thruster forces and moments

The arrangement of the thrusters in the DP system is shown in Fig. 2. Two stern thrusters and two bow thrusters are positioned on the barge, to generate forces to counteract environmental forces. Because the thrusters are installed under the bottom corner of the hull, they can be considered to be in straight running condition. The resultant thrust-induced forces and moments that act on the ship would induce six-DOF motions, and they can be obtained as

$$F_{Tx} = [T_1\cos(\theta_1) + T_2\cos(\theta_2) + T_3\cos(\theta_3) + T_4\cos(\theta_4)]\left(1 - t_p\right) \tag{22}$$

$$F_{Ty} = [T_1\sin(\theta_1) + T_2\sin(\theta_2) + T_3\sin(\theta_3) + T_4\sin(\theta_4)]\left(1 - t_p\right) \tag{23}$$

$$N_{Tx} = \left[-T_1\sin(\theta_1) - T_2\sin(\theta_2) - T_3\sin(\theta_3) - T_4\sin(\theta_4)\right]\left(1 - t_p\right) \times Rd \tag{24}$$

$$N_{Ty} = [T_1\cos(\theta_1) + T_2\cos(\theta_2) + T_4\cos(\theta_4)]\left(1 - t_p\right) \times Rd \tag{25}$$

$$N_{Tz} = [T_1\cos(\theta_1) - T_2\cos(\theta_2) + T_3\cos(\theta_3) - T_4\cos(\theta_4)]\left(1 - t_p\right)\frac{RB}{2} + [T_1\sin(\theta_1) + T_2\sin(\theta_2) - T_3\sin(\theta_3) - T_4\sin(\theta_4)]\left(1 - t_p\right)\frac{RL}{2} \tag{26}$$

where T_1, T_2, T_3, and T_4 are the thrust forces of thrusters 1–4 and θ_1, θ_2, θ_3, and θ_4 are the thrust angles of the thrusters. Because of the simple and low cost requirements of the portable DP system, the control outputs were only the rotation speeds of the thrusters (i.e., n_i in the present simulations) and the thruster angle θ_i was fixed. The parameter t_p is the thrust deduction coefficient, and it was set to 0.06. No cavitation or

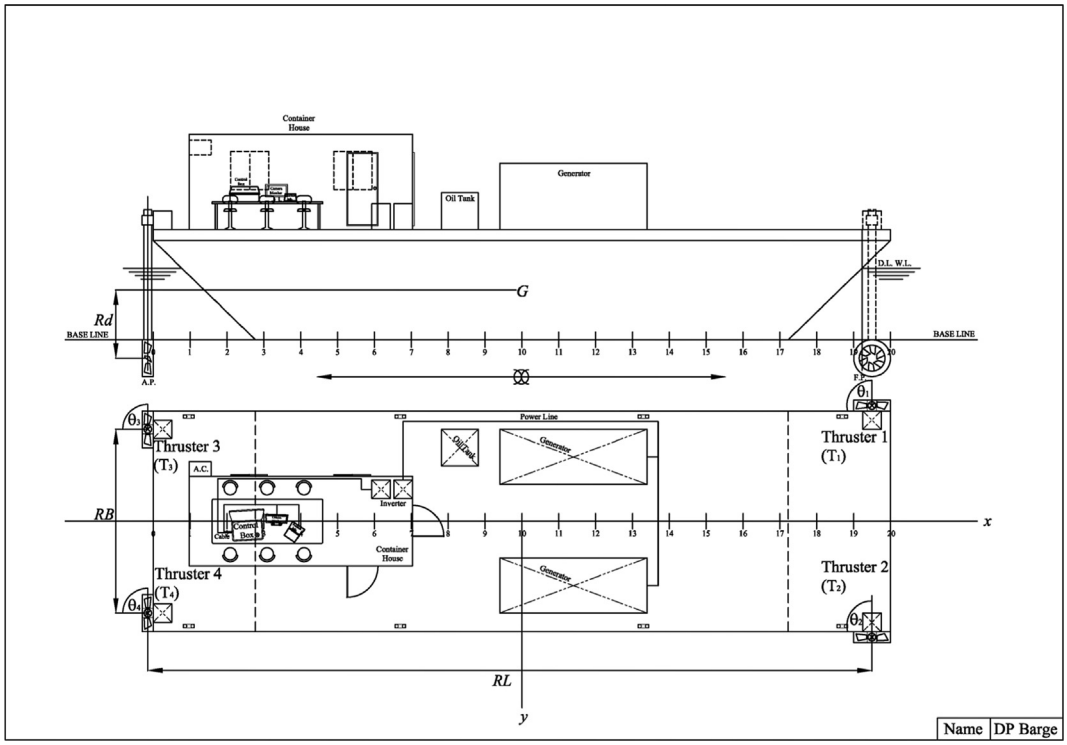

Fig. 2. Arrangement of the four portable thrusters, which were used as the DP system, on the barge.

vibration of the propellers was assumed. The parameter *Rd* is the vertical distance between the center of gravity and the point of thrust, *RB* is the distance between the two stern thrusters, and *RL* is the distance between the two port or starboard thrusters.

To simplify the calculations, the curves K_T (thrust coefficient) and K_Q (torque coefficient) were employed in the first and third quadrants of the plane containing V_A and n_i.

The thrust T_i and propeller torque $Q_{P,i}$, which depend on the effective axial inflow velocity V_A and the propeller rotation speed can be expressed as

$$T_i = \rho n_i |n_i| D_P^4 K_T \tag{27}$$

$$Q_{P,i} = \rho n_i |n_i| D_P^5 K_Q \tag{28}$$

$$\dot{n}_i = \frac{Q_E - |Q_P|}{2\pi(I_{pp} + J_{pp})} \tag{29}$$

$$J = \frac{V_A}{n_i D_p} = \frac{u(1-w_P)}{n_i D_p} \tag{30}$$

$$I_{pp} + J_{pp} = 0.424\rho D_p^5 (2.3) A_E \left(\frac{\pi}{4} D_p^2\right) \tag{31}$$

where ρ, D_P, and J are the water density, propeller diameter, and the advance ratio, respectively, $\dot{n}_i$ is the rate of change of the thruster rotation speed. When the required propeller torque Q_P is larger than the engine torque Q_E, Eq. (29) can be used to adjust the thruster rotation speed. The parameter w_p is the effective propeller wake fraction, and it was set to be 0.1. Furthermore, I_{pp} and J_{pp} are the moment of inertia of the propeller shaft and added moment of inertia of the propeller, respectively, and A_E is the propeller expanded area. Both the blade area ratio A_e/A_o and pitch diameter ratio *P/D* of the propeller were set to 0.7.

8. Control methods for DP system

In the proposed DP system, ship control can be achieved by setting the desired way-points. The desired heading angle that is used to determine the ship heading is obtained using the line-of-sight (LOS) concept and the way-points. The LOS position can be calculated using LOS guidance (Fossen, 2002; Healey and Lienard, 1993). In Fig. 3, the modified LOS position $(X_{los}(t), Y_{los}(t))$ and desired heading angle $\psi_d(t)$ required for heading control are obtained using the following equations:

$$(Y_{los}(t) - Y_G(t))^2 + (X_{los}(t) - X_G(t))^2 = (nL_{pp})^2 \tag{32}$$

$$\frac{Y_{los}(t) - Y_{k-1}(t)}{X_{los}(t) - X_{k-1}(t)} = \frac{Y_k(t) - Y_{k-1}(t)}{X_k(t) - X_{k-1}(t)} = \text{constant.} \tag{33}$$

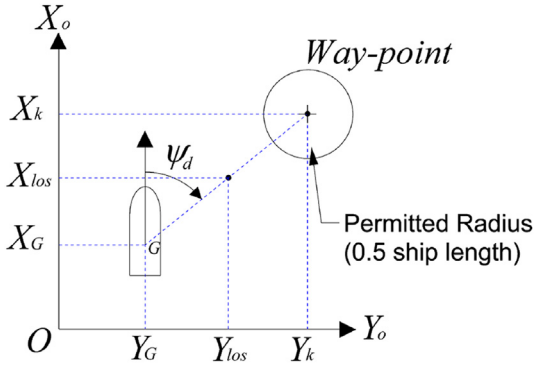

Fig. 3. Modified LOS guidance and a way-point.

$$\psi_d(t) = \tan^{-1}[(Y_{los}(t) - Y_G(t)), (X_{los}(t) - X_G(t))] \tag{34}$$

$$-\pi \le \tan^{-1}[(Y_{los}(t) - Y_G(t)), (X_{los}(t) - X_G(t))] \le \pi \tag{35}$$

$$[Y_k - Y_G(t)]^2 + [X_k - X_G(t)]^2 \le (nL_{pp})^2 \tag{36}$$

where nL_{pp} is the permitted radius (i.e., n times the ship length), (X_k, Y_k) is the present way-point, and $(X_G(t), Y_G(t))$ is the ship position. The point (X_{los}, Y_{los}) can be obtained by solving Eqs. (32) and (33). The four-quadrant inverse tangent function is used in Eqs. (34) and (35). However, the desired heading angle varies with time according to the above coordinates. It is not easy to control the ship so accurately that it passes the way-point precisely under environmental forces. Therefore, in Eq. (36), allowance is made for the way-point to be within a range. When the ship position $(X_G(t), Y_G(t))$ satisfies Eq. (36), (X_{k+1}, Y_{k+1}) can be automatically selected as the next way-point. In other words, when the distance between the ship and the way-point is less than a preset permitted radius ($n = 0.5$ in the present study; in general, $n = 2$ (Fossen, 2002)), the next way-point is selected and the dynamic position system can guide the ship to it. However, if n is set to be too small, it may be difficult for (X_{los}, Y_{los}) to satisfy Eq. (36) in the present DP system. To smooth heading control, the desired heading angle is mapped from $\langle -\pi, \pi \rangle$ to $\langle -\infty, \infty \rangle$ to $\langle 0, 2\pi \rangle$. Details of the mapping procedures can be found in the paper of Breivik (2003).

DP systems based on control theory (i.e., Fig. 4) have been used to control thrusters against environmental forces, for maintaining the ship position and heading.

9. Neuro-fuzzy control algorithm for the DP system

Before describing the architecture of the neuro-fuzzy control algorithm, we provide a brief introduction to a neural network proportional–derivative (PD) controller. Subsequently, the results obtained for the neural network PD controller in the following numerical simulations are compared.

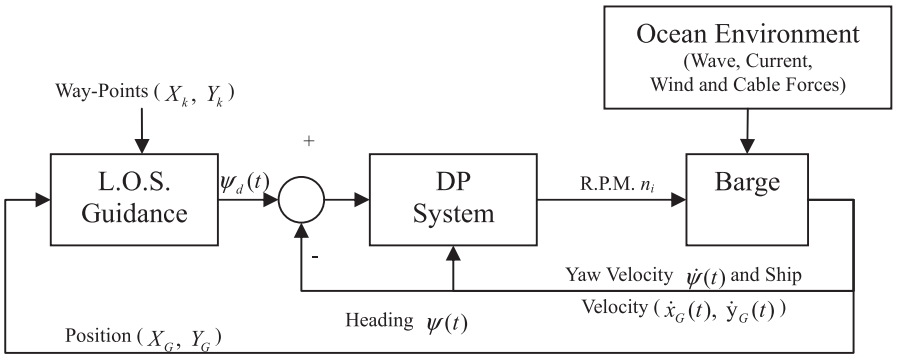

Fig. 4. Control loops of the DP system in the barge.

9.1. Neural network PD controller

The neural network PD control scheme is shown in Fig. 5 (Fang and Lee, 2013), and it consists of two neural network structures:

(i) System identification neural network (*NN1*): The purpose of neural network *NN1* is to find the sensitivity information $\frac{\partial node_{Output,NN1}}{\partial n_i}$, which is the relationship between the ship motion behavior and thruster rotation speed.

The series–parallel model with one hidden layer was adopted in neural network *NN1*, which was applied to identify and predict the nonlinear dynamic relationship between the input and the output. For each ship's x-coordinate (X_G), y-coordinate (Y_G), surge speed (u), sway speed (v), heading deviation ($\psi-\psi_d$), and rotation speeds (n_2, n_3, n_4) of the thrusters (i.e., $X_G(t-1)$, $X_G(t-2)$, $X_G(t-3)$, $Y_G(t-1)$, …, $n_4(t-3)$), 24 nodes were selected as the input nodes of the input layer, and all the input nodes were normalized between −1 and + 1. Fifteen nodes were set in the hidden layer. For the ship's x-coordinate, y-coordinate, surge speed, sway speed, and heading deviation ($\psi-\psi_d$) (i.e., $X'_G(t)$, $X'_G(t-1)$, $X'_G(t-2)$, $Y'_G(t)$, …, $(\psi-\psi_d)'(t-2)$), 15 nodes were set to be the output nodes of the output layer. The error function for *NN1* is defined as

$$E_{NN1} = \frac{1}{2}\left[node_{Input,NN1}(t) - node_{Output,NN1}(t)\right]^2 \tag{37}$$

Because the rotation speeds of the thrusters can be positive or negative (reversion), the hyperbolic tangent function was selected as an adequate activation function:

$$f(x) = \tanh(0.5x) = 2\cdot\left(\frac{1}{1+e^{-x}}\right) - 1 \tag{38}$$

(ii) Parameter self-tuning neural network (*NN2*): The purpose of neural network *NN2* was to obtain the optimal PD control gains for the DP system.

The neural network *NN2* used for tuning the PD control gains was similar to *NN1*; only one hidden layer with fifteen nodes was adopted here. The error function for *NN2* was defined as

$$\begin{aligned} E_{NN2} &= \frac{1}{2}\left[node_{Input,NN2}(t-1) - node_{Input,NN1}(t)\right]^2 \\ &= \frac{1}{2}\left[\Delta node_{Input,NN2}(t-1)\right]^2 \end{aligned} \tag{39}$$

Because the control gains K_P and K_D for dynamic position control are all positive, the sigmoid function with a domain between 0 and 1 was selected as an adequate activation function:

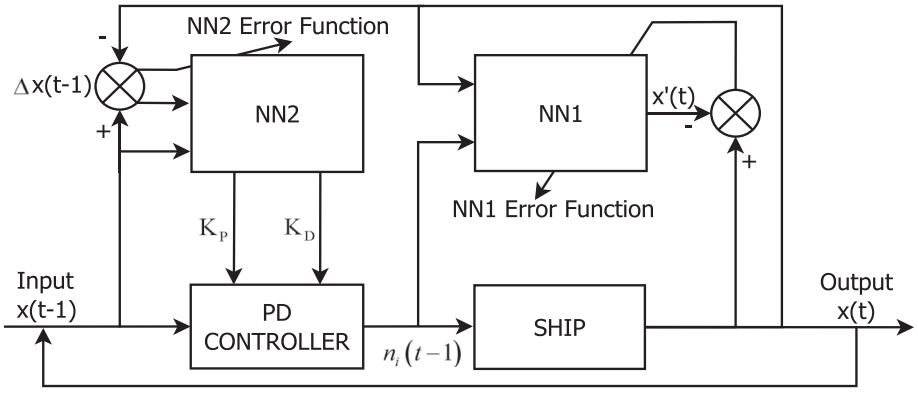

Fig. 5. Control system scheme for the self-tuning neural network PD controller (Fang and Lee, 2013).

$$f(x) = \frac{1}{1+e^{-x}} \tag{40}$$

In the neural network DP control system, only two control gains (i.e., proportion (K_P) and derivation (K_D)) were considered in the PD controller, and the control gain of the integral (K_I) was not considered because the desired goals were fixed and independent of time (i.e., no steady-state error existed in the control system). The use of a back-propagation learning rule for a neural network is actually a general learning example for any smooth parameterized model, including a fuzzy model.

9.2. Neuro-fuzzy control algorithm

A fuzzy DP control system typically has some parameters, such as the rule database and membership function, that are required for the effective operation of the controller. The fuzzy DP control performance is actually affected by "good" or "bad" parameters. For DP control of a sailing ship, appropriate values of the system parameters must be determined. Here, the two parameters in the membership function in Eq. (43) (i.e., $\sigma_{i,j}$ and $x_{bi,j}$) were used to fuzzify the input data, and the $(3 \times j)$ parameters in the rule base ($y_j = p_jX_j+q_jX_j+r_jX_j$) were used for adjusting the fuzzy output. The process used for determining the parameters of the controller was complex and time-consuming. It is not easy to simultaneously adjust most parameters manually. Therefore, this section introduces the neuro-fuzzy control algorithm for the DP system for determining the optimal parameters for different sea states.

The neuro-fuzzy approach provides a method to learn fuzzy modeling from preselected data for fuzzy control. The optimization and adaptation of system parameters into fuzzy rules can be achieved through the learning process of an artificial neural network (ANN).

The fuzzy rules in the "*If-then*" form and the PD controller for the thruster rotation speed were expressed as

$$\textit{If } X_1 \text{ is } a_1,\ X_2 \text{ is } b_1, \text{ and } X_3 \text{ is } c_1, \text{ then } y_1 = p_1X_1 + q_1X_2 + r_1X_3 \tag{41}$$

$$n_j = \left(K_{P,1}X_1 + K_DX_2 + K_{P,2}X_3\right)_j \tag{42}$$

where X_1, X_2, and X_3 are the input vectors, (a_1, b_1, c_1) are linguistic values of the fuzzy set, y_1 is the output vector, and (p_1, q_1, r_1) are the consequent parameters of the rule. In Eq. (41), X_1, X_2, and X_3 are the ship position, velocity, and heading deviations, respectively; $K_{P,1}$, K_D, and $K_{P,2}$ are the jth corresponding control gains of the thruster rotation speed (n_j). Because the output forms in Eqs. (41) and (42) are similar, we can assume that thruster commands with self-tuning control gains are the fuzzy outputs in the neuro-fuzzy DP system. This is a key step in the neuro-fuzzy DP system in the present study.

Fig. 6 illustrates the fuzzy model used in the present study, along with the corresponding neuro-fuzzy layer design. The following five-layer structures were adopted in the neuro-fuzzy algorithm ($O_{1,ij}$ denotes the output of the ith node with the jth member set in layer 1, and $O_{3,k}$ denotes the output of the kth node of layer 3):

(1) Layer 1 of neuro-fuzzy control for the DP system (fuzzifier)

Each node of layer 1 generates a membership function for fuzzifying the input data. For example, the ith node may be a generalized bell-shaped function as follows:

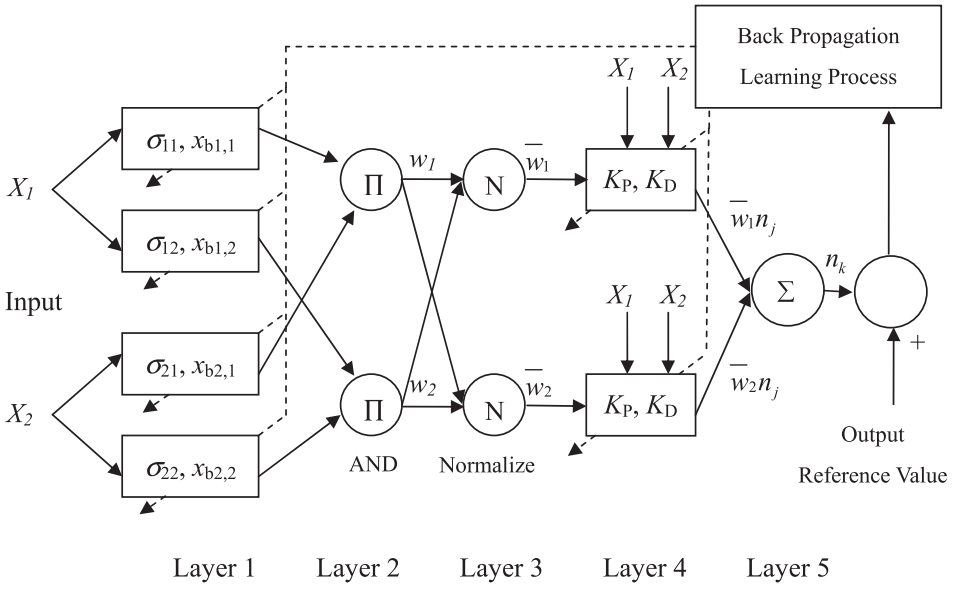

Fig. 6. Five-layer structure of the neuro-fuzzy algorithm.

$$O_{1,ij} = f_{ij}(X_i) = \exp\left[-\left(\frac{X_i - x_{bi,j}}{\sigma_{ij}} \right)^2 \right] \quad i = 1 \sim 10,\ j = 1 \sim 25 \tag{43}$$

where X_i is the scaled input of node i; $f_{ij}(X_i)$ (i.e., the membership function) is the linguistic label (such as small, middle, and large) associated with this node, and $x_{bi,j}$ and σ_{ij} (i.e., the location of maximum function value, and bandwidth) in this layer are referred to as premise parameters.

(2) Layer 2 of neuro-fuzzy control for the DP System (fuzzy inference system)

Each node of layer 2 is the product T-norm operator that multiplies the membership function and sends the product out. For example,

$$O_{2,j} = w(j) = f_{RO(j)}^{(k)} = f_{2i-1,j}(X_{2i-1}) \cdot f_{2i,j}(X_{2i}),\ i = 1 \sim 5;\ j = 1 \sim 25 \tag{44}$$

where $w(j)$ represents the firing strength. The layer can be realized from the corresponding output function based on the jth rule, as part of the operational procedure of fuzzy inference. The application of a back-propagation learning rule to an ANN is actually a general learning example for any smooth parameterized model, including fuzzy inference systems.

(3) Layer 3 of neuro-fuzzy control for the DP system (defuzzifier)

Each node of layer 3 normalizes the rule's firing strength between [0−1].

$$O_{3,k} = \overline{w}(k) = \frac{f_{RO(j)}^{(k)}}{\sum_{j=1}^{25} f_{RO(j)}^{(k)}} = \frac{\prod_{i=2k-1}^{2k} f_{ij}(X_i)}{\sum_{j=1}^{25} \prod_{i=2k-1}^{2k} f_{ij}(X_i)}, \begin{matrix} i = 1 \sim 5 \\ j = 1 \sim 25 \\ k = 1 \sim 5 \end{matrix} \tag{45}$$

The layer can be realized as part of the defuzzifier by using the height defuzzification method.

(4) Layer 4 of neuro-fuzzy control for the DP system (single node output)

The following equation corresponds to each node of layer 4.

$$O_{4,k} = \overline{w}(k) \cdot n_j = \frac{f_{RO(j)}^{(k)}}{\sum_{j=1}^{25} f_{RO(j)}^{(k)}} \cdot n_j = \frac{\prod_{i=2k-1}^{2k} f_{ij}(X_i)}{\sum_{j=1}^{25} \prod_{i=2k-1}^{2k} f_{ij}(X_i)} \cdot \left(K_{P,1}X_1 + K_D X_2 + K_{P,2}X_3\right)_j, \begin{matrix} i = 1 \sim 5 \\ j = 1 \sim 25 \\ k = 1 \sim 5 \end{matrix} \tag{46}$$

where $\overline{w}(j)$ is the output of layer 3, and $(K_{P,1},\ K_D,\ K_{P,2})_j$ are referred to as the consequent parameters in the layer.

(5) Layer 5 of neuro-fuzzy control for the DP system (overall outputs)

The single node outputs in this layer are summarized as the overall outputs:

$$O_{5,k} = \sum_{j=1}^{25} \overline{w}(k) n_j = \frac{\sum_{j=1}^{25} f_{RO(j)}^{(k)} n_j}{\sum_{j=1}^{25} f_{RO(j)}^{(k)}} = \frac{\sum_{j=1}^{25} \prod_{i=2k-1}^{2k} f_{ij}(X_i) \cdot \left(K_{P,1}X_1 + K_D X_2 + K_{P,2}X_3\right)_j}{\sum_{j=1}^{25} \prod_{i=2k-1}^{2k} f_{ij}(X_i)}, \begin{matrix} i = 1 \sim 5 \\ j = 1 \sim 25 \\ k = 1 \sim 5 \end{matrix} \tag{47}$$

Thus, the structures of the five layers of the neuro-fuzzy algorithm are similar to those of a neural network: the first layer is the input layer; the fifth layer is the output layer; and the other layers are regarded as hidden layers in the neural network.

The total number of steps in the five layers of the neuro-fuzzy algorithm is functionally equivalent to a fuzzy inference system. The output $O_{5,k}$ is obtained by using the height-defuzzification method. To determine the practical control requirement, the output values $O_{5,k}$ are scaled into the practical domain (thruster rotation speed).

In the station-keeping mode, only three thrusters are applied: thrusters 2, 3, and 4. The rotations speeds of the thrusters are expressed by the following equations.

$$n_2 = G_{O,3} \cdot O_{5,3} \tag{48}$$

$$n_3 = G_{O,2} \cdot O_{5,2} + G_{O,1} \cdot O_{5,1} \tag{49}$$

$$n_4 = G_{O,2} \cdot O_{5,2} - G_{O,1} \cdot O_{5,1} \tag{50}$$

$$\theta_2 = 90^\circ,\ \theta_3 = \theta_4 = 0^\circ \tag{51}$$

Here, $G_{O,i}(i = 1, 2, 3)$ are the output scaling factors determined by the practical thruster capacities in fuzzy control, n_2 is calculated from $O_{5,3}$ to correct the ship position and velocity deviations in the sway mode, and n_3 and n_4 are calculated from $O_{5,1}$ and $O_{5,2}$ to correct the ship position and velocity deviations in the surge mode and the heading deviation. According to a previous study, controlling the heading by using the sideward thruster (n_2) would increase the sway position deviation because of the large sideward force. However, the two forward thrusters could not produce the required anti-sideward force to correct the sway position deviation. Therefore, control of n_3 and n_4 depends on the surge position and heading deviations, whereas control of n_2 depends only on the sway position deviation.

In the path-tracking mode, all four thrusters are used. The rotation speeds of the thrusters are expressed by the following equations:

$$n_1 = n_2 = G_{O,4} \cdot O_{5,4} \tag{52}$$

$$n_3 = n_4 = G_{O,5} \cdot O_{5,5} \tag{53}$$

$$\theta_1 = \theta_2 = 90^\circ,\ \theta_3 = \theta_4 = 0^\circ \tag{54}$$

where n_1 and n_2 are calculated from $O_{5,4}$ to correct the heading and yaw velocity deviations and n_3 and n_4 are calculated from $O_{5,5}$ to correct the ship position and surge velocity deviations.

9.3. Training process of neuro-fuzzy control algorithm

In this study, in neuro-fuzzy control, a back-propagation learning algorithm was used to adjust the system parameters. The neuro-fuzzy algorithm employs gradient descent to update the premise parameters (i.e., Eqs. (55) and (56)) that define membership functions. The consequent parameters in Eq. (57) provide the coefficients of the output equation. These coefficients can also be obtained by using a neuro-fuzzy algorithm employing the least-squares estimation method. The method is therefore called hybrid learning method (Jang and Sun, 1995) because it combines gradient descent and the least-squares estimation method to adjust the system parameters. When the premise parameters are updated, the consequent parameters are set to be fixed, and vice versa. The learning algorithm constructs a network with the training data, which include the input data (ship position, velocity, and heading deviations) together with the desired thruster rotation speed, and determines how closely the actual network output (thruster rotation speed) matches the desired one. The error function for neuro-fuzzy control (i.e., Eq. (58)) then changes the weight of each connection so that the network produces a better approximation to the desired output. The aforementioned training data are obtained and collected from DP control simulations for different sea states.

$$\begin{aligned}\Delta x_{bi,j} &= \eta_x \frac{\partial E_{NF}}{\partial x_{bi,j}} \\ &= 2\eta_x (n_k - n_{d,k})\overline{w}(k)\left(n_j - n_k\right)\left(\frac{X_i - x_{bi,j}}{\sigma_{ij}^2}\right), \quad \begin{matrix} i = 1 \sim 10, \\ j = 1 \sim 25, \\ k = 1 \sim 5 \end{matrix}\end{aligned} \tag{55}$$

$$\begin{aligned}\Delta \sigma_{ij} &= \eta_\sigma \frac{\partial E_{NF}}{\partial \sigma_{ij}} \\ &= 2\eta_\sigma (n_k - n_{d,k})\overline{w}(k)\left(n_j - n_k\right)\frac{\left(X_i - x_{bi,j}\right)^2}{\sigma_{ij}^3}, \quad \begin{matrix} i = 1 \sim 10, \\ j = 1 \sim 25, \\ k = 1 \sim 5 \end{matrix}\end{aligned} \tag{56}$$

$$\Delta(K_P,\ K_D) = \eta_K \frac{\partial E}{\partial (K_P,\ K_D)} = \eta_K (n_k - n_{d,k})\overline{w}(k),\ \ k = 1 \sim 5 \tag{57}$$

$$E_{NF}(k) = \frac{1}{2}(n_k - n_{d,k})^2, \quad k = 1 \sim 5 \tag{58}$$

where n_k is the thruster rotation speed provided by the neuro-fuzzy network output, $n_{d,k}$ is the desired thruster rotation speed, and η_x, η_σ, and η_K are the learning rates for each parameter correction.

9.4. New control strategy for pipe laying mission

To have highly accurate control at the turning point of a pipe laying route, the DP system should also capture the position and heading. When the ship $(X_G,\ Y_G)$ is very close to the way-point (position deviation is less than 5 m), the DP system changes from the path-tracking mode to the station-keeping mode, and the barge then starts changing the heading to the $k+1$ way-point. When the heading deviation of the $k+1$ way-point is convergent, the barge operates in the path-tracking mode again. The aforementioned techniques are proposed for the DP system based on a neuro-fuzzy algorithm.

10. Results and discussion

A barge model with a portable DP system was selected and its motion behavior on waves was calculated. The neuro-fuzzy control for a DP system described in the previous section was applied in this study. Furthermore, a DP system based on a neural network PD controller was also simulated for comparison.

To meet the DP requirements of a barge, four portable thrusters were used on board, as shown in Fig. 2; the principal dimensions of the barge are presented in Table 1. For simplicity and minimizing portable thrusters, the thruster angle θ_i was set to be fixed. The fourth-order Runge–Kutta method was adopted to solve the six-DOF time-domain simulations of ship motions. The time interval was set to 0.1 s. Before the DP simulation, the parameters ($\sigma_{i,j}$, $x_{bi,j}$, $K_{P,1}$, K_D, and $K_{P,2}$) related to neuro-fuzzy control were stable because the weighting values were trained offline at least 10,000 times (or until the error decreased to 0.001). After the training, the neuro-fuzzy controller could obtain appropriate dynamic parameters for most sea states, which could improve the disadvantage of the trial-and-error method. The system parameters were also adjusted through real-time training in the DP simulations. Four different wave headings, $\psi = 0^\circ$, 180°, 45°, and 90°, were considered. On the basis of regulations laid down by the International Marine Contractors Association, from 2000, the DP system is often set against a scale of a wind force associated with the wind speed, a fixed

Table 1
Principal dimensions of the barge in the DP simulation.

Displacement (tonne)	630.018
Length (m)	30.48
Breadth (m)	9.0
Draft (m)	2.45
Center of gravity above baseline (KG) (m)	4.0
LCG (m)	0
Longitudinal GM (m)	31.85
Transverse GM (m)	0.31
Radius of gyration for pitch (m)	7.62
Radius of gyration for roll (m)	3.15
Water plane area (m^2)	274.32
Distance between stern forward thrusters (m)	5
Wetted surface (m^2)	370.392
Trim (m)	0
Cb	0.9145
Propeller diameter (m)	1.7
Pitch ratio	0.7
Each thruster capacity (kW) (Beaufort scale number = 3)	450

current force, and a wave force along with the corresponding wave height. All three environmental forces act in the same direction, and the relationship between the wind speed and the wave height depends on the sea area. The ITTC-1978 wave spectrum with $H_{1/3} = 0.3\ m$ and $\overline{T} = 2.4$ s (Beaufort scale number 3) was adopted for the simulation conditions. The wind speed and current speed were set to 4.37 m/s and 0.3 m/s, respectively. The original position of the center of gravity was set to be at the origin (0, 0).

The DP trajectories of the barge at $\psi = 45°$ calculated using neural network PD control and neuro-fuzzy control are shown in Fig. 7(a) and (b), respectively. Clearly, both techniques can facilitate DP in an acceptable range, and neuro-fuzzy control appears to be superior. Fig. 8 shows the time histories of the position deviations and the heading deviations. The time histories clearly indicate that neuro-fuzzy control is superior to neural network PD control for position deviations in the X_0 and Y_0 directions and for the maximum heading deviation. Moreover, neuro-fuzzy control stabilizes the heading deviation. The power consumption for neuro-fuzzy control is also less than that for neural network PD control. The maximum forward thrust forces (T_3 & T_4) for neuro-fuzzy control required a compensating thrust force of only 2100 *kgf*, and the sideward thrust force T_2 required a small compensating thrust force of only 250 *kgf*, which demonstrate the effectiveness of the outboard thrusters as a portable DP system. The comparison results are summarized in Table 2, and they clearly indicate that the neuro-fuzzy DP system can constrain the barge to move in a limited acceptable area and is more economical in terms of fuel consumption.

Because neuro-fuzzy (ANFIS) control was found to be superior for DP, it was used to perform pipe-laying work. The trajectory of the barge for neuro-fuzzy control is shown in Fig. 9. Clearly, the barge passed the

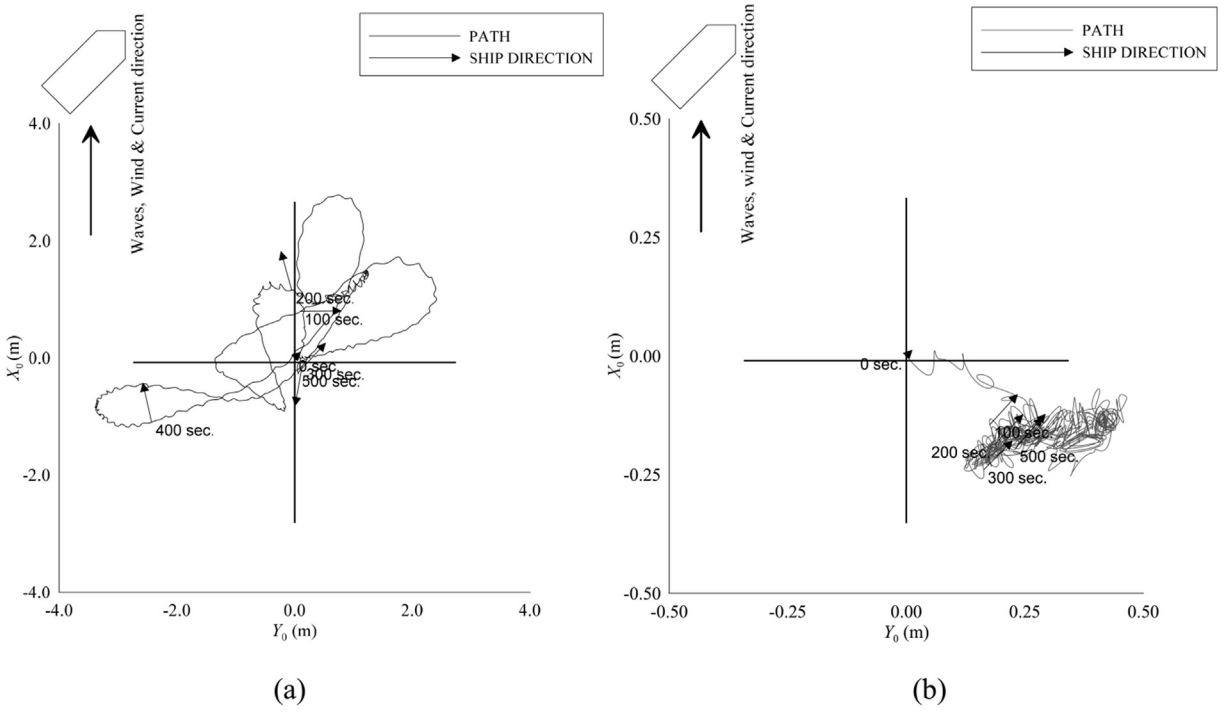

Fig. 7. DP simulation with respect to $\psi = 45°$ using (a) neural network PD control and (b) neuro-fuzzy control for the DP system on short-crested waves (Beaufort scale number = 3; 500 s).

five way-points along the predefined path fairly precisely. The detailed time history of the six-DOF motion response of the ship is shown in Fig. 10. The barge initially sailed smoothly in following sea, which helped maintain the pipe-laying speed at approximately 0.2 m/s. However, the speed increased slightly after passing the way-points. The roll motion appears to vary considerably when the barge sails on oblique waves (i.e., around 500–1000 s and 2000–2500 s), yet the motions are not large. The sway and heave motions appear to show very small fluctuations. Appreciable variations in the yaw motions occur when the barge is approaching and leaving the way-points, and the main reason for this might be the irregular wave effect that caused a large sideward drift. In general, neuro-fuzzy control is found to be suitable for pipe laying on the basis of the simulation.

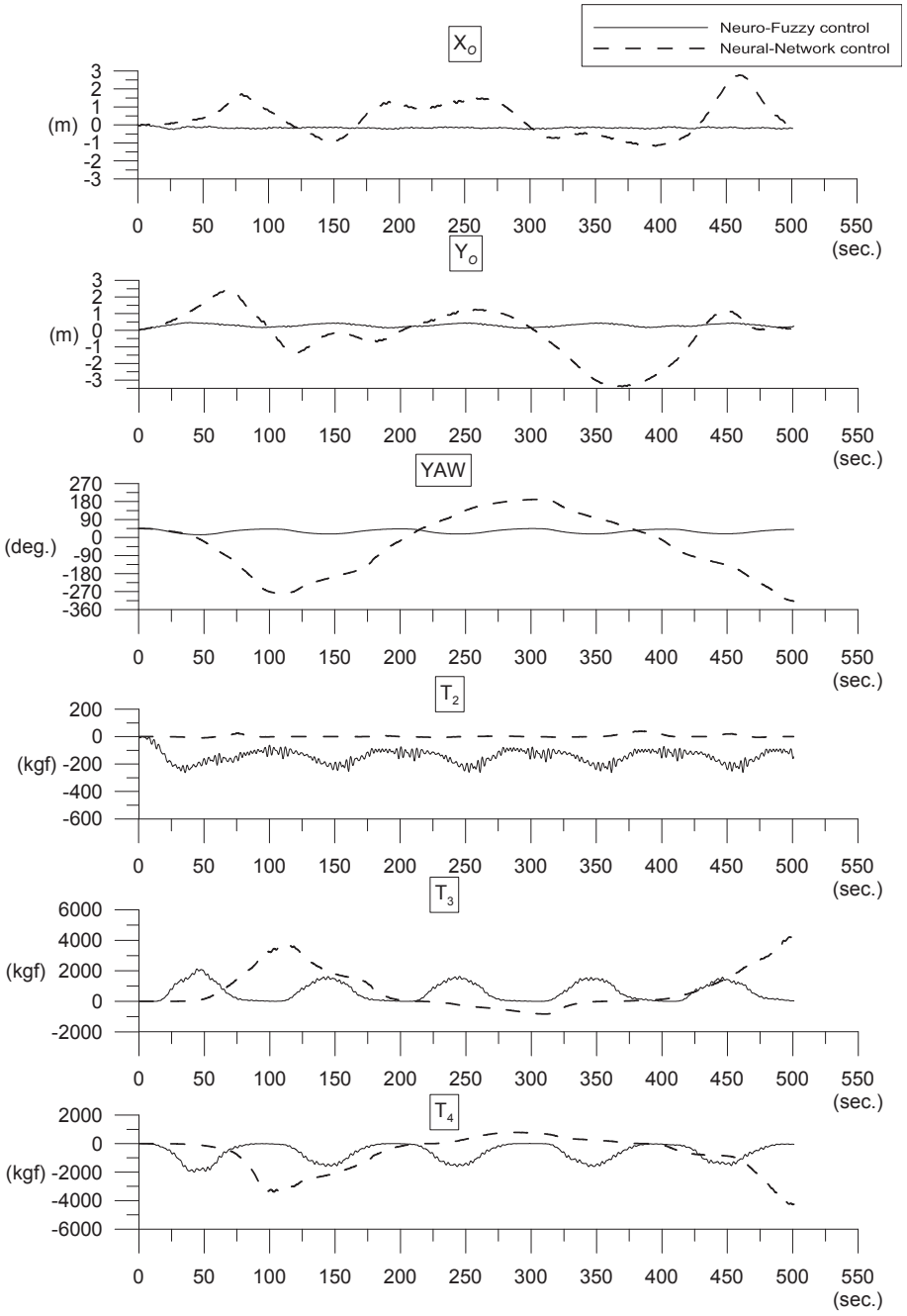

Fig. 8. Time histories of the ship position deviation, heading deviation, and thrust forces for neural network DP control and neuro-fuzzy DP control with respect to $\psi = 45^\circ$ (Beaufort scale number = 3; 500 s).

Table 2
Simulation results for the use of neural network PD control and neuro-fuzzy control in the DP system (Beaufort scale number 3).

Ship heading	$\psi = 180°$	$\psi = 0°$	$\psi = 90°$	$\psi = 45°$
Neural network PD control				
X_0-Position deviation (% of ship length)	6.6%	3.3%	8.2%	9.8%
Y_0-Position deviation (% of ship length)	6.6%	1.6%	12.5%	11.5%
Heading deviation	22°	10°	68°	360°
Max. Thrust T_2	60 *kgf*	10 *kgf*	12.5 *kgf*	35 *kgf*
Max. Thrust T_3 & T_4	2500 *kgf*	900 *kgf*	3000 *kgf*	4000 *kgf*
Neuro-fuzzy control				
X_0-Position deviation (% of ship length)	0.6%	0.7%	1.8%	0.8%
Y_0-Position deviation (% of ship length)	0.6%	0.7%	1.9%	1.6%
Heading deviation	13°	15°	50°	30°
Max. Thrust T_2	50 *kgf*	70 *kgf*	500 *kgf*	250 *kgf*
Max. Thrust T_3 & T_4	600 *kgf*	550 *kgf*	5000 *kgf*	2100 *kgf*

Consequently, we can conclude that the fuzzy logic algorithm performed very well in the pipe-laying mission involving the neuro-fuzzy control system.

11. Conclusion

Simulations of DP of a ship in random waves were performed by using neuro-fuzzy control algorithms and nonlinear motion equations. The results showed that portable outboard thrusters and an appropriate control method can serve as an alternative DP system for controlling vessels without a DP system. The merits of neural networks and fuzzy logic algorithms were combined in the so-called neuro-fuzzy DP system proposed in this study. In a DP system based on the neuro-fuzzy logic algorithm (i.e., ANFIS control), most system parameters can be obtained flexibly through expert knowledge and the parameter self-tuning function. The results show the advantages of this technique for DP control, especially for maintaining the position and heading accurately in oblique and beam seas. The neuro-fuzzy DP system shows the advantages of low position deviation and a small thrust force requirement, simultaneously. In other words, the neuro-fuzzy DP system can achieve high-efficiency control in most conditions. However, the present methodology for a nonconventional portable-type DP control system is only a theoretical model. When the DP control system is operated in practice, the sensor signal treatment with a Kalman filter and the thruster power lag are critical aspects that should be carefully considered.

In summary, for many ocean engineering cases, the portable DP system developed in this study can serve as a practical and economical tool for assisting ships lacking a DP system. Among the different control methods for DP systems discussed in this paper, the neuro-fuzzy algorithm is recommended for pipe-laying missions.

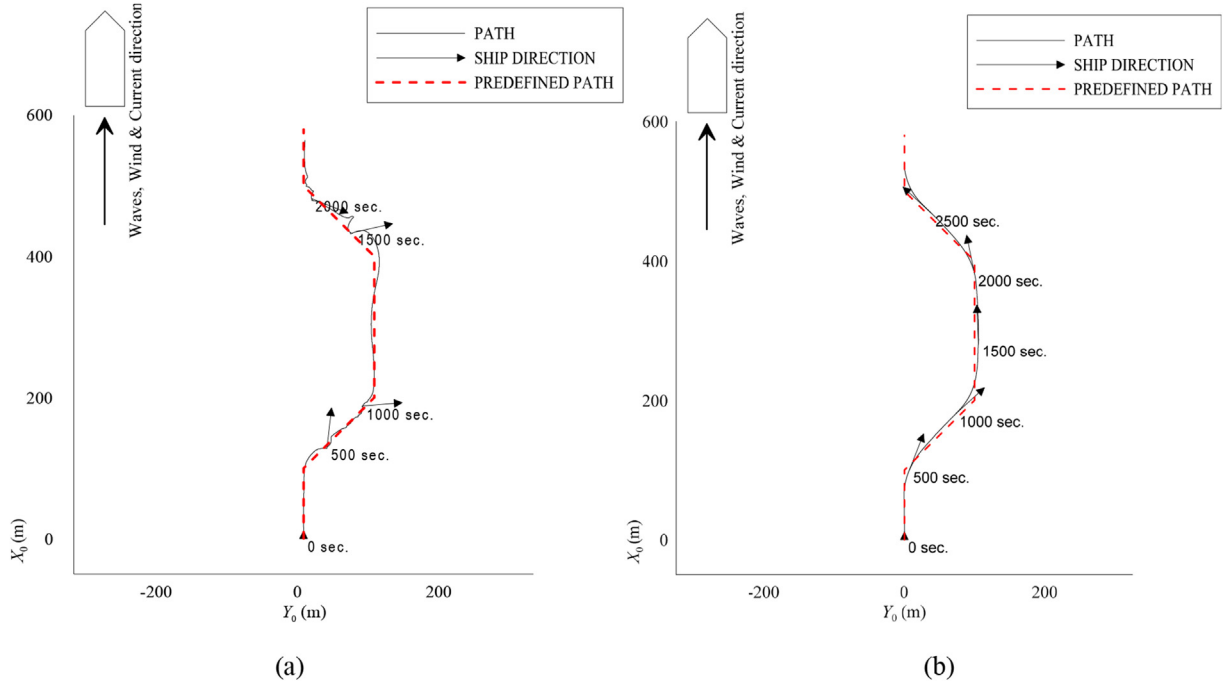

Fig. 9. Ship trajectory for 2900 s; path-tracking simulation involving (a) neural network PD control and (b) neuro-fuzzy control in the DP system (Beaufort scale number = 3).

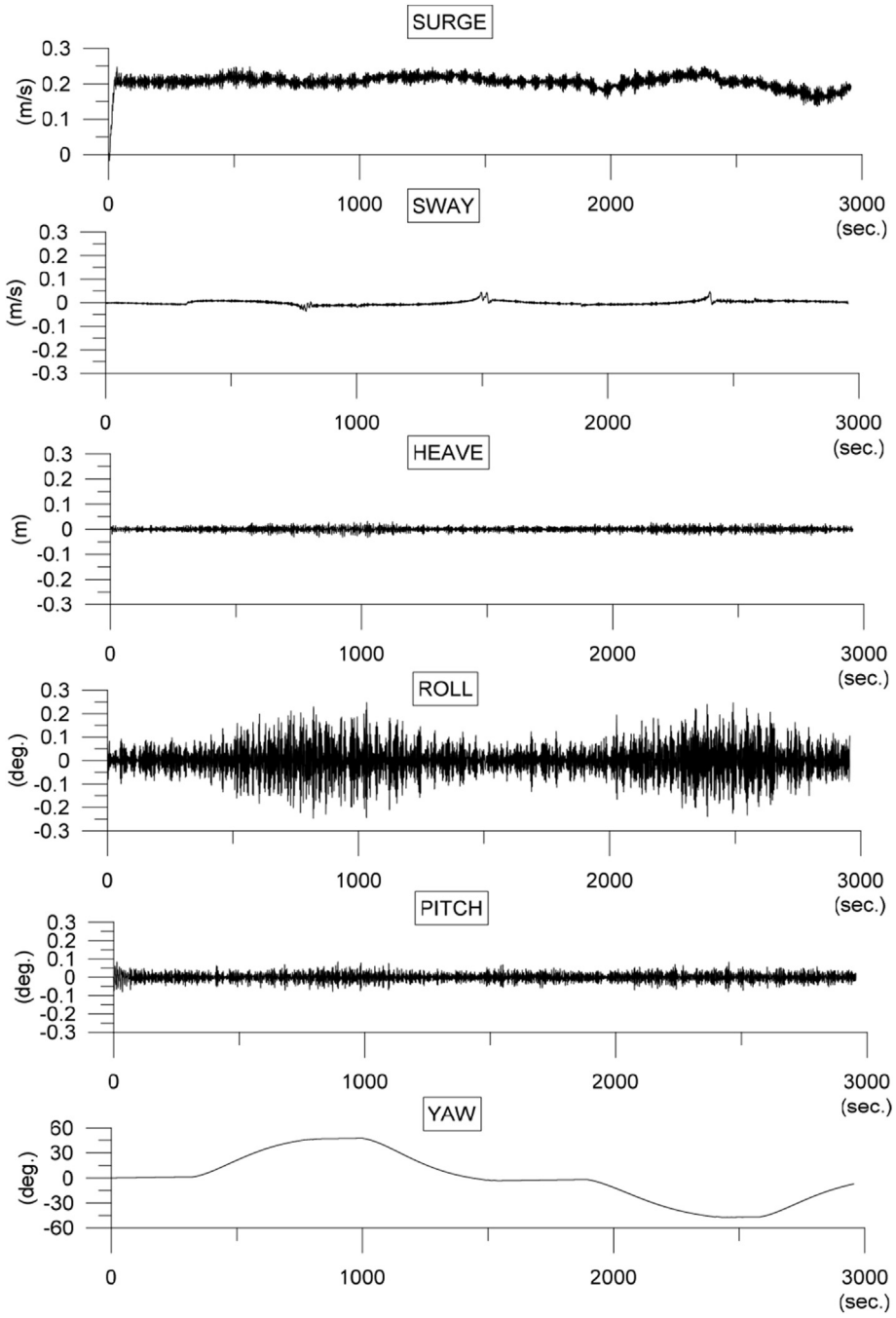

Fig. 10. Ship motion response during the 2900 s path-tracking simulation involving neuro-fuzzy control in the DP system (Beaufort scale number = 3).

Acknowledgments

The authors thank the International Wave Dynamics Research Center, National Cheng Kung University, Taiwan, for providing financial support (No. MOST 104-2911-I-006). Financial support from the Research Center for Energy Technology and Strategy, NCKU, is also acknowledged.

References

Balchen, J.G., Jenssen, N.M., Mathisen, E., Salid, S., 1980. A dynamic positioning system based on Kalman filtering and optimal control. MIC 1 (3), 135–163.

Breivik, M., 2003. Nonlinear Maneuvering Control of Underactuated Ships. Master thesis. Norwegian University of Science and Technology.

Cheng, Yuan Chung, 2000. The Application of the Self-tuning Fuzzy Controller Based on the Adaptive Network on the Pump System. Master

thesis(in Chinese). Department of Mechanical Engineering, National Central University, Taoyuan, Taiwan.

Crossland, P., Johnson, M.C., 1998. A time domain simulation of deck wetness in head seas. In: Proceeding of RINA International Conference on Ship Motions and Manoeuverability, London, UK.

Fang, M.-C., 1991. Second-order steady forces on a ship advancing in waves. Int. Shipbuild. Prog. 38 (413), 73–93.

Fang, M.-C., Lee, M.L., Lee, C.K., 1993. The simulation of water shipping for a ship advancing in large longitudinal waves. J. Ship Res. 37, 26–137.

Fang, M.-C., Lee, Z.-Y., 2013. Portable dynamic positioning control system on a barge in short-crested waves using the neural network algorithm. China Ocean Eng. 27 (4), 469–480.

Fang, M.-C., Lee, Z.-Y., Huang, K.-T., 2013. A simple alternative approach to assess the effect of the above-water bow form on the ship added resistance. Ocean Eng. 57, 34–48.

Fang, M.-C., Luo, J.-H., 2005. The nonlinear hydrodynamic model for simulating a ship steering in waves with autopilot system. Ocean Eng. 32 (11–12), 1486–1502.

Fay, H., 1989. Dynamic Positioning Systems, Principles, Design and Applications(France: Editions). Technip, Paris.

Fossen, T.I., 2002. Marine control Systems: Guidance, Navigation and Control of Ships, Rigs and Underwater Vehicles, first ed. Marine Cybernetics, Trondheim, Norway.

Hamamoto, M., Matsuda, A., Ise, Y., 1994. Ship motion and the dangerous zone of a ship in severe following seas(in Japanese). J. Soc. Nav. Archit. Jpn. 175, 69–78.

Healey, A.J., Lienard, D., 1993. Multivariable sliding-mode control for autonomous diving and steering of unmanned underwater vehicles. IEEE J. Ocean. Eng. 18 (3), 327–339.

Isherwood, R.M., 1973. Wind resistance of merchant ships. Trans. RINA 115, 327–338.

ITTC, 2005. Recommended procedures and guidelines, recommendations of ITTC for parameters. Rev. 02. In: The International Towing Tank Conference.

Jang, J.S.R., Sun, C.-T., 1995. Neuro-fuzzy modeling and control. Proc. IEEE 83 (3), 378–406.

Lee, T.H., Cao, Y.S., Lin, Y.M., 2002. Dynamic positioning of drilling vessels with a fuzzy logic controller. Int. J. Syst. Sci. 33 (12), 979–993.

Luo, Jhih-Hong, 2001. Directional Stability and Motions of a Ship in Severe Following Waves. Master thesis(in Chinese). Department of Naval Architecture and Marine Engineering, National Cheng Kung University, Tainan, Taiwan.

Luo, Jhih-Hong, 2006. The Study on the Maneuvering and Control of the Nonlinear Ship Motions in Waves. PhD dissertation(in Chinese). Department of Systems and Naval Mechatronic Engineering, National Cheng Kung University, Tainan, Taiwan.

Maritime Reporter, 2002. Creating a Portable Dynamic Positioning System, Maritime Reporter and Engineering News. January issue, p. 46.

Michel, W.H., 1999. Sea spectra revisited. Mar. Technol. 36 (4), 211–227.

Morgan, M.J., 1978. Dynamic Positioning of Offshore Vessels. Petroleum Publishing Co., Tulsa ,Oklahoma.

Nienhuis, Ir U., 1986. Simulation of Low Frequency Motions of Dynamically Positioned Offshore Structures, vol. 129. The Royal Institution of Naval Architects, pp. 127–145.

Perez, T., Donaire, A., 2009. Constrained control design for dynamic positioning of marine vehicles with control allocation. Model. Identif. Control 30 (2), 57–70.

Phelps, B.P., 1995. Ship Structural Response Analysis: Spectra and Statistics, Defence Science and Technology Organisation Technical Report: DSTO-TR-0183. Aeronautical and Maritime Research Laboratory, Melbourne.

Saelid, S., Jenssen, N.A., Balchen, J.G., 1983. Design and analysis of a dynamic positioning system based on Kalman filtering and optimal control. IEEE Trans. Autom. Control 28 (3), 331–339.

Salvesen, N., 1974. Second-order steady state forces and moments on surface ships in oblique regular waves. In: Int. Symp. On Dynamics of Marine Vehicles and Structures in Waves, London, pp. 212–227.

Sørensen, A.J., Sagatun, S.I., Fossen, T.I., 1996. Design of a dynamic positioning system using model-based control. J. Control Eng. Pract. 4 (3), 359–368.

Sørensen, A.J., 2011. A survey of dynamic positioning control systems. Annu. Rev. Control 35 (1), 123–136.

Tannuri, E.A., Donha, D.C., 2000. H_∞ controller design for dynamic positioning of turret moored FPSO. In: In Proceedings of the IFAC Conference on Manoeuvring and Control of Marine Craft. Denmark, Aalborg.

The International Marine Contractors Association, 2000. Specification for DP Capability Plots. IMCA, M140 Rev. 1.

Zalewski, P., 2011. Path following problem for a DP ship simulation model. TransNav Int. J. Mar. Navig. Saf. Sea Transp. 5 (1), 111–117.